CrystEngComm

RSC Publishing

PAPER

View Article Online
View Journal | View Issue

Competing hydrogen-bond and halogen-bond donors in crystal engineering†

Cite this: *CrystEngComm*, 2013, **15**, 3125

Christer B. Aakeröy,* Sheelu Panikkattu, Prashant D. Chopade and John Desper

In order to study the structure-directing competition between hydrogen- and halogen-bond donors we have synthesized two ligands, 3,3′-azobipyridine and 4,4′-azobipyridine, and co-crystallized them with a series of bi-functional donor molecules comprising an activated halogen-bond donor (I or Br) as well as a hydrogen-bond donor (acid, phenol or oxime) on the same backbone. Based on the subsequent single-crystal analysis, 5 of 6 co-crystals of 3,3′-azobipyridine are assembled using hydrogen bonds as the primary driving force accompanied by weaker secondary (C–X···O) interactions. However, in 5 out of the 6 co-crystals of 4,4′-azobipyridine, both hydrogen bonds (O–H···N) and halogen bonds (C–X···N) are present as structure-directing interactions leading to 1-D chains. Since the charges on the acceptor sites in 3,3′- and 4,4′-azobipyridine are very similar, the observed difference in binding behaviour highlights the importance of binding-site location on the acceptor molecules (*anti*-parallel in 3,3′-azobipyridine and co-linear in 4,4′-azobipyridine) as a direct influence over the structural balance between hydrogen- and halogen-bond donors.

Received 23rd October 2012,
Accepted 27th November 2012

DOI: 10.1039/c2ce26747k

www.rsc.org/crystengcomm

Introduction

Many hydrogen-bond based synthons[1] such as acid···pyridine,[2] acid···amide,[3] phenol···pyridine,[4] oxime···N(heterocycle)[5] have been explored extensively as robust and reliable tools for crystal engineering and supramolecular synthesis. Recently, halogen bonds,[6] which play important roles in areas such as biochemistry,[7] medicinal chemistry,[8] and material science,[9] have found uses in crystal engineering because these interactions have properties that parallel those of hydrogen bonds in terms of directionality and strength.[10,11] Typical hydrogen-bond strengths range from approximately 4–60 kJ mol^{-1},[12] while halogen bonds range from 5–180 kJ mol^{-1} (the strong interaction I_2···I^- in I_3^- is the extreme).[13] Consequently, iodine/bromine, suitably 'activated' through a fluorinated backbone, should be capable of competing with hydrogen bonds in a supramolecular reaction.[14]

The combination of hydrogen bonds (HBs) and halogen bonds (XBs) is gaining importance in crystal engineering,[15] and in order to investigate the structure-directing balance between HBs and XBs we decided to employ a set of bi-functional donor molecules equipped with one HB donor and one XB donor attached to the same molecular backbone; 4-iodotetrafluorobenzoic acid (COOH-I), 4-bromotetrafluorobenzoic acid (COOH-Br), 4-iodotetrafluorophenol (OH-I), 4-bromotetrafluorophenol (OH-Br), 4-iodotetrafluoroaldoxime (Ox-I) and 4-bromotetrafluoroaldoxime (Ox-Br) (Scheme 1). These probe molecules were subsequently co-crystallized with two isomeric symmetric acceptors 3,3′- and 4,4′-azobipyridine (3,3′-azpy and 4,4′-azpy, respectively) (Scheme 1).

In this study, we investigate the following:

1) Competition between HB and XB donors for the pyridine nitrogen atoms which are capable of forming both hydrogen bonds and halogen bonds (Scheme 2).

2) Possible influence of geometric differences of the donors and acceptors on the competition and overall structural outcome.

3) Participation of auxiliary potential acceptors like carbonyl oxygen atoms, hydroxyl oxygen atoms and azo nitrogen atoms (Scheme 3) in weaker interactions with halogen atoms.

In Scheme 2, we have outlined the postulated structural outcomes of the co-crystallizations as a function of the relative strength and supramolecular efficiency of HB *vs.* XB in this series of co-crystallizations.

It is well known that electrostatic charge is important for predicting or rationalizing molecular recognition events,[16] but in this study, the two acceptor molecules have rather similar electrostatic potentials of interaction as indicated by the values of −174 and −172 kJ mol^{-1} for 3,3′-azpy and 4,4′-azpy respectively, corresponding to the minima in the molecular electrostatic potential surface (0.002 e au^{-1}) determined using a positive charge in vacuum as the probe after optimizing their molecular geometries using DFT (B3LYP) with a 6-31++G** basis set. There is therefore no real charge-based 'bias'

Department of Chemistry, Kansas State University, Manhattan, KS, 66506, USA. E-mail: aakeroy@ksu.edu

† Electronic supplementary information (ESI) available: Details of the synthesis of compounds. CCDC 906983–906994. For ESI and crystallographic data in CIF or other electronic format see DOI: 10.1039/c2ce26747k

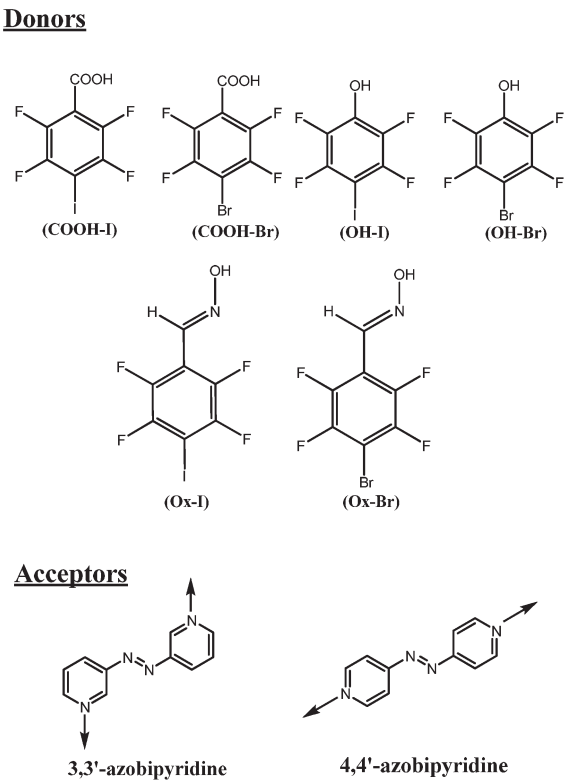

Scheme 1 Bi-functional donors and isomeric symmetric acceptors.

between the two acceptors. However, there is a geometric difference since the binding sites differ in their relative orientation, *i.e.* in case of 3,3′-azpy, the pyridine nitrogen atoms are aligned anti-parallel whereas in 4,4′-azpy they are co-linear with respect to each other (Scheme 1). It is conceivable that this difference may affect the primary molecular recognition events, which can subsequently lead to the formation of distinctly different supramolecular assemblies.

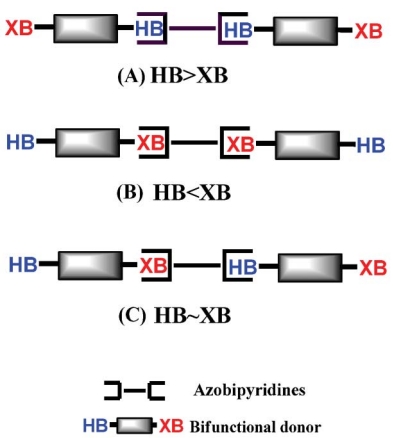

Scheme 2 Postulated outcomes.

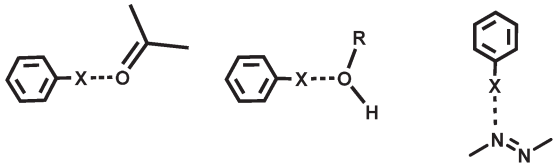

Scheme 3 Potential secondary interactions between halogen atoms, X, and suitable electron-pair donors.

Experimental set up

A library of six bifunctional halogen–hydrogen bond donors and two symmetric acceptors (Scheme 1) was employed. 3,3′-Azobipyridine and 4,4′-azobipyridine,[17] 4-iodotetrafluorobenzoic acid and 4-bromotetrafluorobenzoic acid[18] were synthesised as reported. 4-Iodotetrafluorophenol was synthesised from iodopentafluorobenzene using potassium hydroxide in *tert*-butanol (see ESI†). 4-Iodotetrafluoroaldoxime and 4-bromotetrafluoroaldoxime were synthesised in one-step from their corresponding 4-halotetrafluoroaldehydes *via* a green solvent-assisted grinding method.[19] Synthesis of all the HB–XB donors is included in the ESI.† 4-Bromotetrafluorophenol was purchased from Sigma Aldrich. The donors and acceptors were combined in stoichiometric amounts giving a total of 12 co-crystal combinations, Table 1. Single crystals were obtained upon slow evaporation of the solvent, and we were able to obtain crystals suitable for single-crystal diffraction for products from all twelve reactions.

X-Ray crystallography

Datasets were collected on a Bruker SMART APEX II system with Mo radiation (**3,3′-azpy:COOH-I**, **3,3′-azpy:OH-I**) **3,3′-azpy:OH-Br**, **3,3′-azpy:Ox-I**, **3,3′-azpy:Ox-Br**, **4,4′-azpy:COOH-I**, **4,4′-azpy:OH-Br**, **4,4′-azpy:Ox-I** or a Bruker Kappa APEX II system with Cu radiation (**3,3′-azpy:COOH-Br**, **4,4′-azpy:COOH-Br**, **4,4′-azpy:OH-I**, **4,4′-azpy:Ox-Br**) at 120 K using APEX2 software.[20] An Oxford Cryostream 700 low-temperature device was used to control temperature. Initial cell constants were found by small widely separated ''matrix'' runs. Data collection strategies were determined using COSMO.[21] Scan speeds and scan widths were chosen based on scattering power and peak rocking curves.

Unit-cell constants and orientation matrices were improved by least-squares refinement of reflections threshold from the entire dataset. Integrations were performed with SAINT,[22] using these improved unit cells as a starting point. Precise unit cell constants were calculated in SAINT from the final merged datasets. Lorenz and polarization corrections were applied. Absorption corrections was applied using SADABS.[23]

Datasets were reduced with SHELXTL.[24] The structures were solved by direct methods without incident. Coordinates for all oxime and phenol hydrogen atoms were allowed to refine. All other hydrogen atoms were assigned to idealized positions and were allowed to ride. Isotropic thermal parameters for the hydrogen atoms were constrained to be 1.5× (methyl)/1.2× (all other) that of the connected atom.

Table 1 Synthesis of 3,3′- and 4,4′-azobipyridine co-crystals

Acceptors	Donors	Co-crystal abbreviation	Mole ratio	Solvent/method	Melting points, °C
3,3′-Azobipyridine	4-Iodotetrafluorobenzoicacid	**3,3′-azpy:COOH-I**	1 : 1	Ethanol/slow evaporation	182–185
	4-Bromotetrafluorobenzoicacid	**3,3′-azpy:COOH-Br**	1 : 1	Ethanol/slow evaporation	155–157
	4-Iodotetrafluorophenol	**3,3′-azpy:OH-I**	1 : 1	Ethanol/slow evaporation	125–127
	4-Bromotetrafluorophenol	**3,3′-azpy:OH-Br**	1 : 1	Ethanol/slow evaporation	170–173
	4-Iodotetrafluoroaldoxime	**3,3′-azpy:O*x*-I**	1 : 1	Ethanol/slow evaporation	145–148
	4-Bromotetrafluoroaldoxime	**3,3′-azpy:O*x*-Br**	1 : 1	Ethanol/slow evaporation	105–108
4,4′-Azobipyridine	4-Iodotetrafluorobenzoicacid	**4,4′-azpy:COOH-I**	1 : 1	Ethanol/slow evaporation	220–222
	4-Bromotetrafluorobenzoicacid	**4,4′-azpy:COOH-Br**	1 : 1	Ethanol/slow evaporation	190–191
	4-Iodotetrafluorophenol	**4,4′-azpy:OH-I**	1 : 1	Ethanol/slow evaporation	163–165
	4-Bromotetrafluorophenol	**4,4′-azpy:OH-Br**	1 : 1	Ethanol/slow evaporation	133–136
	4-Iodotetrafluoroaldoxime	**4,4′-azpy:O*x*-I**	1 : 1	Ethanol/slow evaporation	115–116
	4-Bromotetrafluoroaldoxime	**4,4′-azpy:O*x*-Br**	1 : 1	Ethanol/slow evaporation	125–126

3,3′-azpy:COOH-I. Two orientations for the haloacid were located, in roughly head-to-tail positions. Geometry for the two components was restrained to similarity by using the SHELXL ''SAME'' command. Thermal parameters of closely located atoms were pairwise constrained using the SHELXL ''EADP'' command. Coordinates of the ammonium hydrogen atom H11 were allowed to refine.

3,3′-azpy:COOH-Br. Coordinates for the carboxylic acid hydrogen atom H21 were allowed to refine.

3,3′-azpy:OH-I. Coordinates for the carboxylic acid hydrogen atom H21 were allowed to refine.

3,3′-azpy:OH-Br. Coordinates for the phenol hydrogen atoms H31 and H41 were allowed to refine.

3,3′-azpy:O*x*-I. Coordinates for the oxime hydrogen atom H27 were allowed to refine.

3,3′-azpy:O*x*-Br. Coordinates for the oxime hydrogen atom H17 were allowed to refine

4,4′-azpy:COOH-I. The sample was a racemic twin, and populations of the two components were parameterized using the SHELXL ''TWIN'' and ''BASF'' commands. Two orientations for the haloacid were located, in roughly head-to-tail positions. Geometry for the two components was restrained to similarity by using the SHELXL ''SAME'' command. Thermal parameters of closely located atoms were pairwise constrained using the SHELXL ''EADP'' command. Thermal parameters for the nearly inversion-related pyridines N11–C16 and N21–C26 were also constrained using the ''EADP'' command, and these thermal parameters were restrained to approximately the same values using the SHELXL ''SIMU'' command. The ammonium hydrogen atom H11 was placed in an idealized geometry and allowed to ride on its parent nitrogen atom.

4,4′-azpy:COOH-Br. The asymmetric unit contains two acid–base pairs, each of which was assigned to a SHELXL RESI due for consistent labelling purposes. Two orientations for each halo acid were located, in roughly head-to-tail positions. Similarly, two closely related orientations for the amine were found. Geometry for all four acid components was restrained to similarity by using the SHELXL ''SAME'' command. Geometry for all four base components was also restrained to similarity by using the SHELXL ''SAME'' command. Thermal parameters of closely located atoms were pairwise constrained using the SHELXL ''EADP'' command.

4,4′-azpy:OH-I. The phenol hydrogen atom H31 was placed in an idealized geometry and allowed to ride on its parent oxygen atom.

4,4′-azpy:OH-Br. Coordinates for the phenol hydrogen atom H11 were allowed to refine.

4,4′-azpy:O*x*-I. Coordinates for the oxime hydrogen atom H37 were allowed to refine.

4,4′-azpy:O*x*-Br. Coordinates for the oxime hydrogen atom H27 were allowed to refine.

Selected hydrogen and halogen-bond geometries are shown in Tables 2 and 3 respectively. The crystallographic parameters of 3,3′- and 4,4′-azobipyridine co-crystals are listed in Tables 4 and 5, respectively.

Results

Co-crystals of 3,3′-azobipyridine

3,3′-Azobipyridine:4-iodotetrafluorobenzoic acid. The crystal structure determination of **3,3′-azpy:COOH-I** shows that the result is a neutral molecular solid with two acid molecules for every one bipy. The co-crystal is formed *via* two symmetry related O–H···N hydrogen bonds between one carboxylic acid and a nitrogen atom, Table 2. These interactions lead to trimeric supermolecules which are subsequently connected into 2-D corrugated sheets *via* C–I···$O_{(C=O)}$ contacts (Fig. 1).

3,3′-Azobipyridine:4-bromotetrafluorobenzoic acid. In the **3,3′-azpy:COOH-Br** co-crystal, the primary driving force is a pair of acid-pyridine O–H···N hydrogen bonds which produce neutral trimers that are further extended into 2-D sheets *via* C–Br···$O_{(C=O)}$ interactions (Fig. 2).

3,3′-Azobipyridine:4-iodotetrafluorophenol. 4-Iodotetrafluorophenol has two potential single point donors, *i.e.* I and OH that could potentially bind to the nitrogen atoms. In **3,3′-azpy:OH-I** however, hydroxyl hydrogen atom interacts with the nitrogen atoms in symmetry related O–H···N hydrogen bonds leading to a trimeric supermolecule. These trimers are then further connected into 2-D sheets *via* weaker C–I···$O_{(C=O)}$ interactions (Fig. 3).

3,3′-Azobipyridine:4-bromotetrafluorophenol. In the **3,3′-azpy:OH-Br** co-crystal, intermolecular O–H···N hydrogen bonds direct the formation of primary trimeric building blocks. The interaction of the bromine atom with a hydroxyl

Table 2 Hydrogen-bond geometries in co-crystals of 3,3′- and 4,4′-azobipyridine[a]

Compound	D–H···A/Å	D–H/Å	H···A/Å	D···A/Å	D–H···N/°
3,3′-azpy:COOH-I	N(11)–H(11)···O(21A)_#1	1.22(2)	1.32(2)	2.536(2)	174(2)
3,3′-azpy:COOH-Br	O(21)–H(21)···N(11)_#1	1.14(3)	1.41(3)	2.549(2)	177(3)
3,3′-azpy:OH-I	O(21)–H(21)···N(11)_#1	0.90(2)	1.75(2)	2.6162(15)	159(2)
3,3′-azpy:OH-Br	O(31)–H(31)···N(11)	0.88(2)	1.77(2)	2.6224(16)	163.2(18)
	O(41)–H(41)···N(21)	0.88(2)	1.73(2)	2.5963(15)	166.8(18)
3,3′-azpy:O*x*-I	O(27)–H(27)···N(27)_#1_#2	0.72(2)	2.18(2)	2.8460(17)	153(2)
3,3′-azpy:O*x*-Br	O(17)–H(17)···N(21)_#1	0.76(4)	1.95(4)	2.708(3)	178(4)
4,4′-azpy:COOH-I	N(11)–H(11)···O(31B)_#1	0.88	1.75	2.605(9)	164.3
		0.88	1.73	2.598(6)	167.5
4,4′-azpy:COOH-Br	O31A1–H31A1···N11A1	0.84	1.76	2.566(10)	158.8
	O31B1–H31B1···N21B1_#1	0.84	1.84	2.67(3)	167.6
	O31A2–H31A2···N11A2	0.84	1.75	2.587(9)	170.0
	O31B2–H31B2···N21B2_#2	0.84	1.83	2.67(4)	175.3
4,4′-azpy:OH-I	O(31)–H(31)···N(11)	0.84	1.84	2.614(4)	152.3
4,4′-azpy:OH-Br	O(31)–H(31)···N(11)	0.83(2)	1.86(2)	2.6342(16)	155(2)
4,4′-azpy:O*x*-I	O(37)–H(37)···N(11)	0.82(2)	1.90(2)	2.7052(19)	169(2)
4,4′-azpy:O*x*-Br	O(27)–H(27)···N(11)_#1	0.94(6)	1.79(6)	2.704(6)	162(6)

[a] Symmetry codes: **3,3′-azpy:COOH-I** #1 $-x-1, -y, -z+2$. **3,3′-azpy:COOH-Br** #1 $-x+2, -y+1, -z$. **3,3′-azpy:OH-I** #1 $-x+1, -y+1, -z+1$. **3,3′-azpy:O*x*-I** #1 $-x, -y, -z+2$; #2 $-x+3, -y+1, -z$. **3,3′-azpy:O*x*-Br** #1 $-x, -y, -z-1$. **4,4′-azpy:COOH-I** #1 $x+2, y-2, z+1$. **4,4′-azpy:COOH-Br** #1 $x-1, y+1, z+1$; #2 $x+2, y+1, z+1$. **4,4′-azpy:O*x*-Br** #1 $-x+2, -y+3, -z+1$.

oxygen lone pair links neighbouring trimers into 2-D assemblies (Fig. 4).

3,3′-Azobipyridine:4-iodotetrafluoroaldoxime. In the co-crystal of **3,3′-azpy:O*x*-I**, iodine atoms form C–I···N halogen bonds with the two pyridine nitrogen atoms, while the oxime participates in a self-complementary dimer (Fig. 5). This results in a 1-D non-planar corrugated chain-like assembly with the donor and acceptor molecules aligned almost perpendicular to each other. Among all the co-crystals of 3,3′-azobipyridine with bifunctional donor molecules, this is the only example in which halogen bonds (not hydrogen bonds) are present as the primary mode of interaction.

3,3′-Azobipyridine:4-bromotetrafluoroaldoxime. The structure of **3,3′-azpy:O*x*-Br** shows aldoxime hydrogen atoms interacting with pyridine *via* symmetry related O–H···N hydrogen bonds, while the aldoxime oxygen atom interacts with bromine in a C–Br···O contact producing a 2-D layer (Fig. 6).

Co-crystals of 4,4′-azobipyridine

4,4′-Azobipyridine:4-iodotetrafluorobenzoic acid. In the **4,4′-azpy:COOH-I** co-crystal, intermolecular O–H···N hydrogen bonds and C–I···N halogen bond interactions produce infinite 1-D chain-like assemblies as the primary supramolecular motifs (Fig. 7).

4,4′-Azobipyridine:4-bromotetrafluorobenzoic acid. The **4,4′-azpy:COOH-Br** co-crystal contains infinite 1-D chains formed *via* intermolecular O–H···N hydrogen bonds and near-linear C–Br···N halogen bonds (Fig. 8).

4,4′-Azobipyridine:4-iodotetrafluorophenol. In the **4,4′-azpy:OH-I** co-crystal, both the hydroxyl hydrogen atom and the iodine atom bind to a pyridine nitrogen atom, resulting in an infinite 1-D chain (Fig. 9).

Table 3 Halogen-bond geometries in co-crystals of 3,3′- and 4,4′-azobipyridine[a]

Compound	C–X···A	X···A/Å	C–X···A/°
3,3′-azpy:COOH-I	C–(24A)–I(1)···O(22A)_#2	2.8694(13)	170.66(6)
3,3′-azpy:COOH-Br	C–(24)–Br(1)···O(22)_#2	2.8792(17)	172.23(7)
3,3′-azpy:OH-I	C(24)–I(1)···O(21)_#2	3.0913(10)	156.81(4)
3,3′-azpy:OH-Br	C(34)–Br(1)···O(31)_#1	3.1138(11)	156.32(5)
	C(44)–Br(2)···O(41)_#2	3.0750(10)	158.68(5)
3,3′-azpy:O*x*-I	C(24)–I(1)···N(11)	2.8279(12)	174.75(4)
3,3′-azpy:O*x*-Br	C(14)–Br(1)···O(17)_#1	3.0557(19)	158.49(9)
4,4′-azpy:COOH-I	C(34A)–I(1A)···N(21)_#1	2.796(5)	173.4(3)
4,4′-azpy:COOH-Br	C(34A1)–Br(1A1)···N(21A1)_#1	2.802(7)	176.9(4)
4,4′-azpy:OH-I	C(34)–I(1)···N(21)_#1	2.960(3)	165.98(11)
4,4′-azpy:OH-Br	C(34)–Br(1)···N(21)_#1	2.9717(12)	165.95(5)
4,4′-azpy:O*x*-I	C(34)–I(1)···N(21)_#1	2.8200(15)	178.38(5)
4,4′-azpy:O*x*-Br	C(24)–Br(1)···N(14)_#1	3.395(4)	171.94(17)

[a] Symmetry codes **3,3′-azpy:COOH-I** #2 $x+1, -y+1/2, z-1/2$. **3,3′-azpy:COOH-Br** #2 $x-1, -y+1/2, z+1/2$. **3,3′-azpy:OH-I** #2 $-x+1/2, y-1/2, -z+3/2$. **3,3′-azpy:OH-Br** #1 $-x+1, y-1/2, -z+1/2$; #2 $-x, y+1/2, -z+3/2$. **3,3′-azpy:O*x*-Br** #1 $x, y+1, z+1$. **4,4′-azpy:COOH-I** #1 $x-2, y+2, z-1$. **4,4′-azpy:COOH-Br** #1 $x-1, y+1, z+1$. **4,4′-azpy:OH-I** #1 $x-2, y+1, z+1$. **4,4′-azpy:OH-Br** #1 $x+2, y-1, z-1$. **4,4′-azpy:O*x*-I** #1 $x-1/2, -y-1/2, z+1/2$. **4,4′-azpy:O*x*-Br** #1 $x-1/2, -y+3/2, z-1/2$.

Table 4 Crystallographic parameters of 3,3′-azobipyridine co-crystals

	3,3′-azpy:COOH-I	3,3′-azpy:COOH-Br	3,3′-azpy:OH-I	3,3′-azpy:OH-Br	3,3′-azpy:O*x*-I	3,3′-azpy:O*x*-Br
Formula moiety	$(C_{10}H_8N_4)$ $(C_7HF_4IO_2)_2$	$(C_{10}H_8N_4)$ $(C_7HBrF_4O_2)_2$	$(C_{10}H_8N_4)$ $(C_6HF_4IO)_2$	$(C_{10}H_8N_4)$ $(C_6HBrF_4O)_2$	$(C_{10}H_8N_4)$ $(C_7H_2F_4INO)_2$	$(C_{10}H_8N_4)$ $(C_7H_2BrF_4NO)_2$
Empirical formula	$C_{24}H_{10}F_8I_2N_4O_4$	$C_{24}H_{10}Br_2F_8N_4O_4$	$C_{22}H_{10}F_8I_2N_4O_2$	$C_{22}H_{10}Br_2F_8N_4O_2$	$C_{24}H_{12}F_8I_2N_6O_2$	$C_{24}H_{12}Br_2F_8N_6O_2$
Molecular weight	824.16	730.18	768.14	674.16	822.20	728.22
Color, habit	Orange rod	Orange plate	Orange plate	Orange prism	Orange prism	Orange plate
Crystal system	Monoclinic	Monoclinic	Monoclinic	Monoclinic	Triclinic	Triclinic
Space group, *Z*	$P2_1/c$, 2	$P2_1/c$, 2	$C2/c$, 4	$P2_1/c$, 4	$P\bar{1}$, 1	$P\bar{1}$, 1
a, Å	4.9020(3)	4.8724(3)	19.0228(11)	18.2149(8)	5.6341(4)	8.3500(8)
b, Å	21.4561(12)	22.0007(13)	16.8636(10)	16.4379(7)	10.4834(7)	8.3646(8)
c, Å	12.1298(7)	11.6936(7)	7.2425(4)	7.4736(4)	11.5197(8)	9.8996(10)
α, °	90.00	90.00	90.00	90.00	75.365(2)	105.765(3)
β, °	100.151(2)	101.336(3)	93.198(2)	99.631(2)	77.562(2)	103.151(3)
γ, °	90.00	90.00	90.00	90.00	80.975(2)	99.733(3)
Volume, Å^3	1255.82(13)	1229.06(13)	2319.7(2)	2206.17(18)	639.09(8)	628.00(11)
X-Ray wavelength	0.71073	1.54178	0.71073	0.71073	0.71073	0.71073
μ, mm^{-1}	2.606	5.151	2.806	3.774	2.556	3.325
Absorption corr	Multi-scan	Multi-scan	Multi-scan	Multi-scan	Multi-scan	Multi-scan
Trans min/max	0.4893/0.8186	0.5657/0.7531	0.4671/0.8497	0.3602/0.4906	0.4951 0.7161	0.4159/0.8255
Reflections Collected	13 823	7259	18 196	62 309	15 760	10 635
Independent	4126	2158	3957	7628	4637	3773
Observed	3713	2046	3666	6276	4497	3174
Threshold expression	$>2\sigma(I)$	$>2\sigma(I)$	$>2\sigma(I)$	$>2\sigma(I)$	$>2\sigma(I)$	$>2\sigma(I)$
R_1 (observed)	0.0207	0.0261	0.0176	0.0265	0.0186	0.0480
wR_2 (all)	0.0508	0.0688	0.0463	0.0699	0.0444	0.1288
S	1.064	1.084	1.021	0.998	1.085	1.052

4,4′-Azobipyridine:4-bromotetrafluorophenol. The **4,4′-azpy:OH-Br** co-crystal displays 1-D infinite chains formed *via* intermolecular O–H···N hydrogen bonds and C–Br···N halogen bonds (Fig. 10).

4,4′-Azobipyridine:4-iodotetrafluoroaldoxime. In the **4,4′-azpy:O*x*-I** co-crystal, 1-D infinite zig-zag chains are constructed *via* hydrogen (O–H···N) and halogen (C–I···N) bonds (Fig. 11).

4,4′-Azobipyridine:4-bromotetrafluoroaldoxime. Unlike in the previous structures, in the **4,4′-azpy:O*x*-Br** structure, the aldoxime hydrogen atoms form oxime···pyridine hydrogen bonds on both sides of the acceptor, while bromine on the other end interacts with the azo nitrogen (C–Br···$N_{(azo)}$, 3.397 Å) (Fig. 12). The bond distance is longer than a typical C–Br···$N_{aromatic}$ halogen bond (Aver. 3.04 Å), but slightly shorter than the sum of their (Br and N) van der Waals radii

Table 5 Crystallographic parameters of 4,4′-azobipyridine co-crystals

	4,4′-azpy:COOH-I	4,4′-azpy:COOH-Br	4,4′-azpy:OH-I	4,4′-azpy:OH-Br	4,4′-azpy:O*x*-I	4,4′-azpy:O*x*-Br
Formula moiety	$(C_{10}H_8N_4)$ $(C_7HF_4IO_2)$	$(C_{10}H_8N_4)$ $(C_7HBrF_4O_2)$	$(C_{10}H_8N_4)$ (C_6HF_4IO)	$(C_{10}H_8N_4)$ (C_6HBrF_4O)	$(C_{10}H_8N_4)$ $(C_7H_2F_4INO)$	$(C_{10}H_8N_4)$ $(C_7H_2BrF_4NO)_2$
Empirical formula	$C_{17}H_9F_4IN_4O_2$	$C_{17}H_9BrF_4N_4O_2$	$C_{16}H_9F_4IN_4O$	$C_{16}H_9BrF_4N_4O$	$C_{17}H_{10}F_4IN_5O$	$C_{24}H_{12}Br_2F_8N_6O_2$
Molecular weight	504.18	457.19	476.17	429.18	503.20	728.22
Color, habit	Bronze plate	Orange prism	Orange plate	Colourless plate	Orange plate	Orange needle
Crystal system	Triclinic	Triclinic	Triclinic	Triclinic	Monoclinic	Monoclinic
Space group, *Z*	$P1$, 1	$P\bar{1}$, 4	$P\bar{1}$, 2	$P\bar{1}$, 2	$C2/c$, 8	$P2_1/n$, 2
a, Å	6.2112(8)	10.1607(5)	6.1515(5)	6.3706(3)	17.6282(7)	10.2846(10)
b, Å	8.1879(11)	13.4553(6)	9.8197(7)	9.5670(5)	6.3167(3)	4.6215(5)
c, Å	8.9824(12)	14.4474(8)	13.7443(10)	13.3289(7)	31.7318(14)	27.841(2)
α, °	84.843(3)	112.158(3)	81.558(3)	79.453(2)	90.00	90.00
β, °	70.837(3)	90.592(3)	85.932(3)	83.090(2)	96.518(2)	98.246(6)
γ, °	77.402(3)	111.504(3)	78.342(3)	79.4760(10)	90.00	90.00
Volume, Å^3	421.03(10)	1676.48(14)	803.57(10)	782.03(7)	3510.6(3)	1309.6(2)
X-Ray wavelength	0.71073	1.54178	1.54178	0.71073	0.71073	1.54178
μ, mm^{-1}	1.967	3.967	16.211	2.687	1.884	4.795
Absorption corr	Multi-scan	Multi-scan	Multi-scan	Multi-scan	Multi-scan	Multi-scan
Trans min/max	0.5544/0.9255	0.5354/0.7420	0.1813/0.5633	0.5804/0.7464	0.6401/0.9284	0.5662/0.7531
Reflections Collected	8655	18 301	11 713	17 166	27 187	7830
Independent	4606	5840	2764	5315	6206	2257
Observed	4415	5035	2604	4829	5308	1721
Threshold expression	$>2\sigma(I)$	$>2\sigma(I)$	$>2\sigma(I)$	$>2\sigma(I)$	$>2\sigma(I)$	$>2\sigma(I)$
R_1 (observed)	0.0433	0.0851	0.0275	0.0269	0.0239	0.0595
wR_2 (all)	0.1149	0.2211	0.0756	0.0720	0.0575	0.1586
S	1.062	1.038	1.082	1.037	1.040	1.099

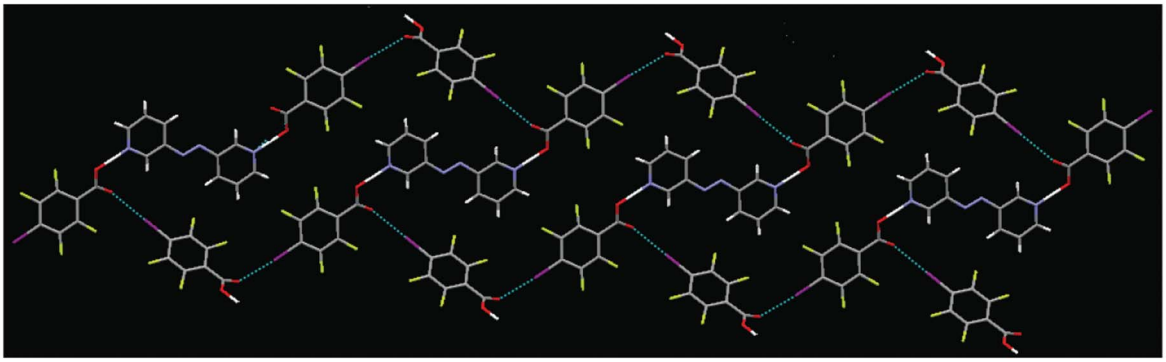

Fig. 1 2-D network formed *via* strong O–H···$N_{(py)}$ and weaker C–I···$O_{(C=O)}$ interactions in the **3,3′-azpy:COOH-I** co-crystal. The apparent 'covalent' bond between COOH and py is due to a disorder over two positions of the haloacid.

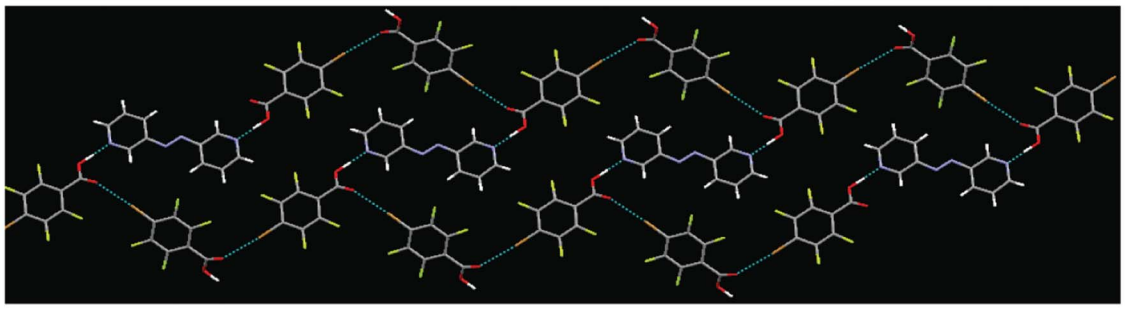

Fig. 2 3,3′-azpy:COOH-Br co-crystal showing primary O–H···$N_{(py)}$ and secondary C–Br···$O_{(C=O)}$ interactions.

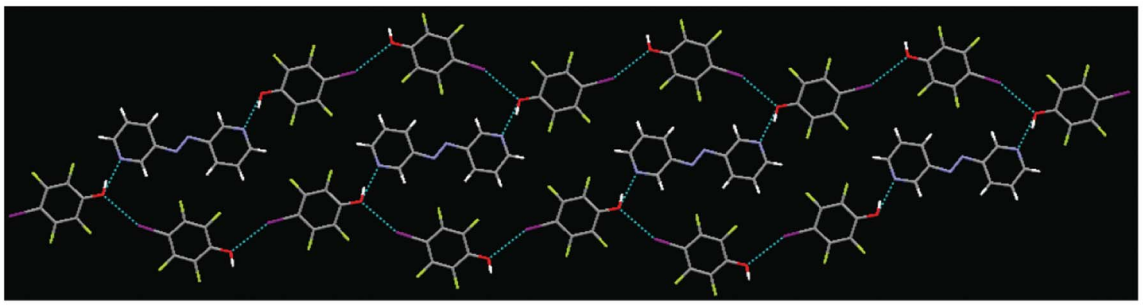

Fig. 3 3,3′-azpy:OH-I crystal structure showing primary O–H···$N_{(py)}$ and secondary C–I···$O_{(C=O)}$ interactions forming an eight component repeat unit.

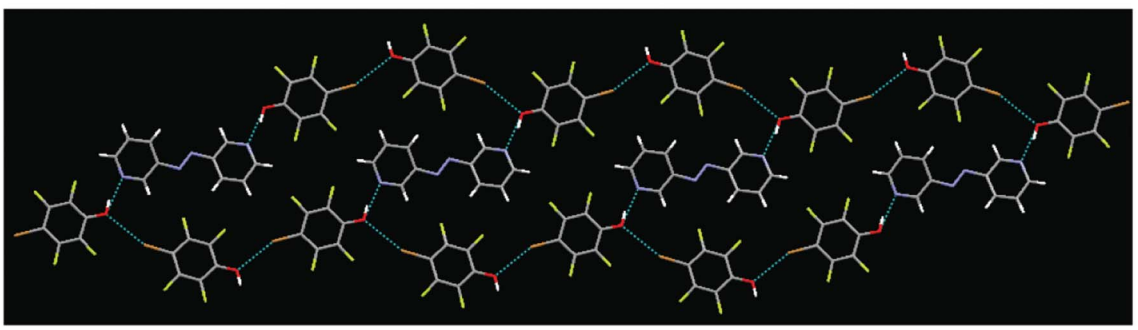

Fig. 4 3,3′-azpy:OH-Br crystal structure showing intermolecular O–H···$N_{(py)}$ and C–Br···O interactions forming the multi-component supermolecule.

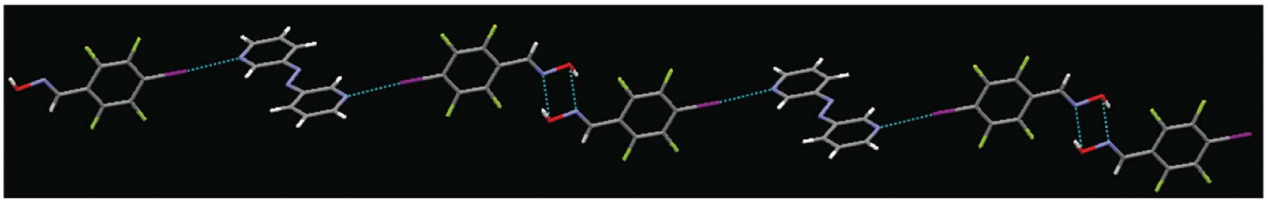

Fig. 5 3,3′-azpy:Ox-I co-crystal with oxime–oxime dimer and C–I···$N_{(py)}$ halogen bonds forming 1-D non-planar corrugated chain.

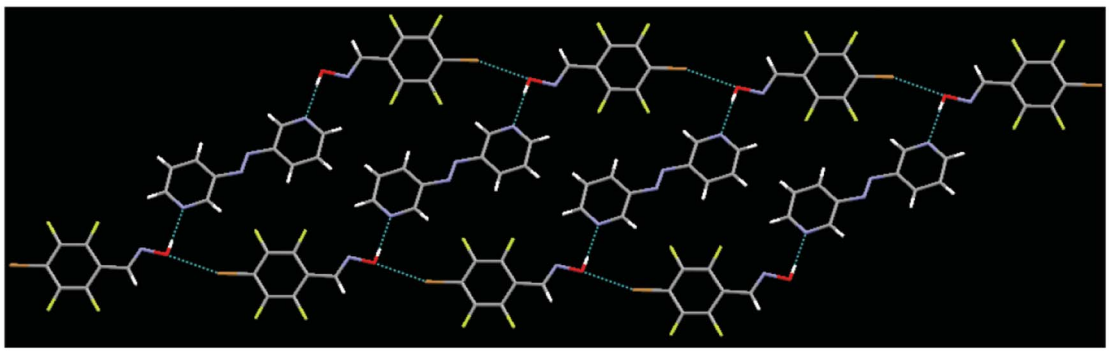

Fig. 6 3,3′-azpy:Ox-Br crystal structure showing O–H···$N_{(py)}$ primary hydrogen bonds and secondary C–Br···O interactions.

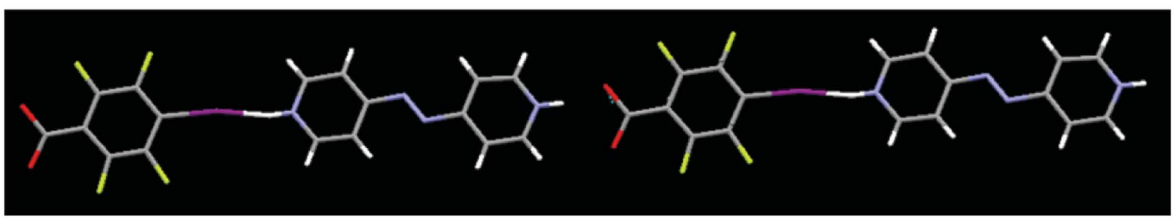

Fig. 7 1-D infinite chain in **4,4′-azpy:COOH-I** co-crystal formed *via* O–H···$N_{(py)}$ and C–I···$N_{(py)}$ hydrogen and halogen bond, respectively. For specific information about the crystallography, see the Experimental section.

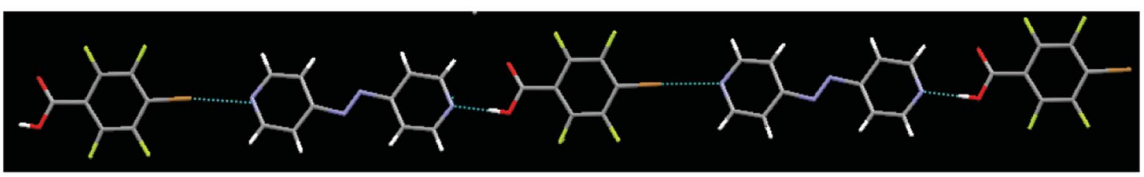

Fig. 8 4,4′-azpy:COOH-Br co-crystal showing primary O–H···$N_{(py)}$ hydrogen bonds and C–Br···$N_{(py)}$ halogen-bond interactions.

(3.40 Å). Although there are very few examples of the halogen-bonding ability of azo-nitrogen atoms this Br···$N_{(azo)}$ interaction aligns the azobipyridine almost perpendicular to the plane, leading to a 3-D architecture, Fig. 13.

Discussion

Twelve co-crystallizations were performed using two isomeric pyridine-based acceptors (3,3′- and 4,4′-azobipyridine) and six bi-functional donors comprising both a HB donor (acid, phenol and oxime) as well as an XB donor (iodine and bromine) on the same backbone. Single-crystal structural data were acquired for solids obtained from all 12 reactions. The primary interactions driving the crystal assembly were the O–H···$N_{(py)}$ hydrogen bonds or C–X···$N_{(py)}$ halogen bonds followed by secondary interactions which were used to connect the primary motifs. In all co-crystals, there were several potential acceptors *e.g.* N(py), N(azo), O(–O=C) and O(–OH), and donors *e.g.* acid, phenol, oxime, iodine and bromine. Considering the

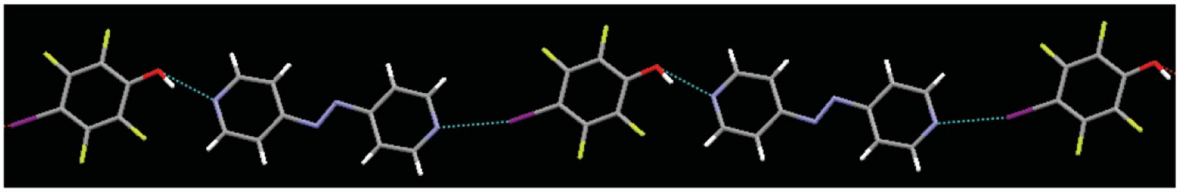

Fig. 9 4,4′-azpy:OH-I crystal structure with 1-D chains formed *via* both O–H···$N_{(py)}$ and C–I···$N_{(py)}$ interactions.

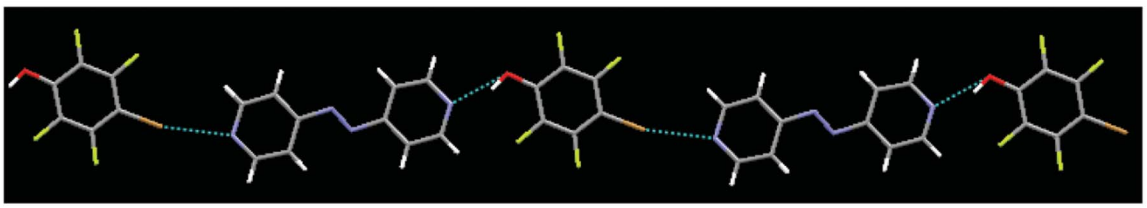

Fig. 10 The **4,4′-azpy:OH-Br** co-crystal contains 1-D chains formed by both hydrogen (O–H···$N_{(py)}$) and halogen (C–Br···$N_{(py)}$) bonds.

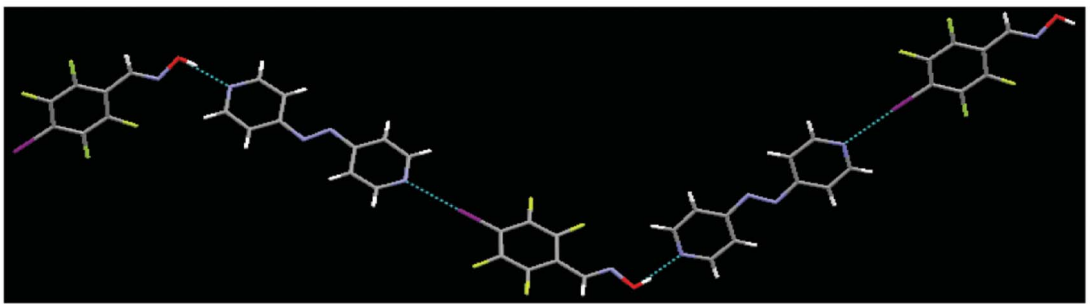

Fig. 11 Part of the crystal structure of **4,4′-azpy:Ox-I** with C–I···$N_{(py)}$ and O–H···$N_{(py)}$ interactions forming a 1-D chain.

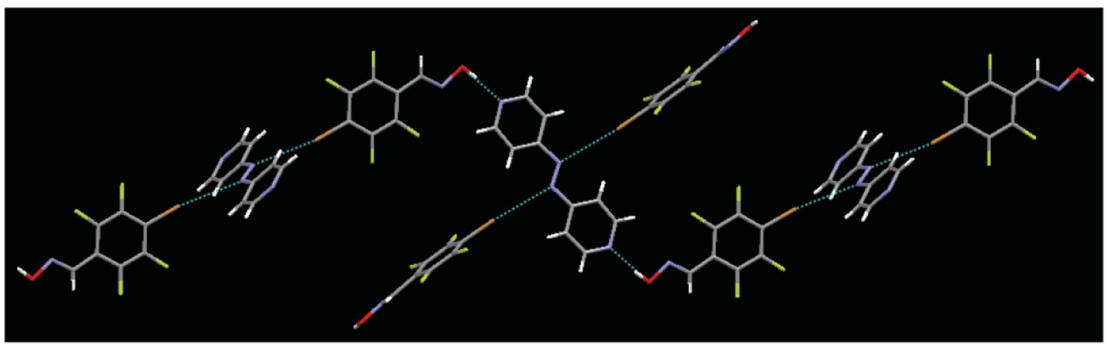

Fig. 12 Part of the **4,4′-azpy:Ox-Br** crystal structure with O–H···$N_{(py)}$ hydrogen bonds and C–Br···$N_{(azo)}$ interactions.

complexity of such a system, and although it was reasonable to expect some degree of structural 'chaos' in the supramolecular outcome, we observe remarkable consistency in the binding pattern within the two classes of acceptors. Table 6 and Scheme 4 summarize the structural landscape in these twelve crystal structures.

Data from the Cambridge Structural Database (CSD) were used to compare both O···N as well as X···N (X = I/Br) intermolecular bond distances. The search in CSD was limited to aromatics alone. The average O···N bond distances reported for acid–pyridine (381 hits), phenol–pyridine (435 hits) and aldoxime–pyridine (7 hits) are 2.63 Å, 2.74 Å and 2.71 Å respectively; while for our crystal structures the corresponding values are 2.60 Å, 2.62 Å and 2.71 Å. Based on the values obtained from CSD, the O···N bond distance decreases in the following order, phenol–pyridine > oxime–pyridine > acid–

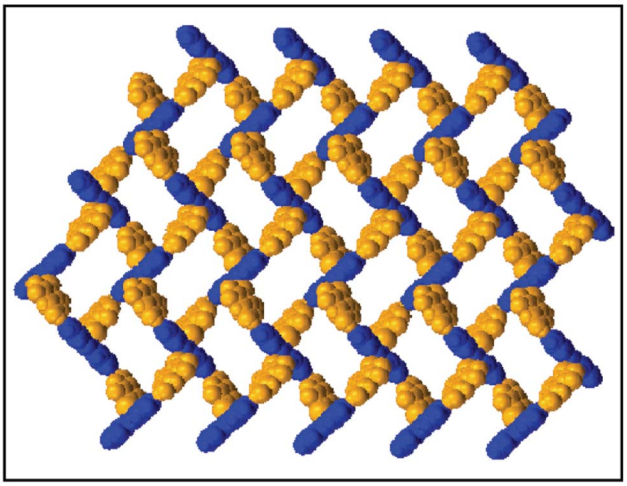

Fig. 13 3D-architecture in the **4,4-′azpy:O*x*-Br** co-crystal.

pyridine. However our study shows the following trend, oxime–pyridine > phenol–pyridine > acid–pyridine. The discrepancy observed in the order between oxime and phenol could be due to the limited number of crystal structure data (7 hits) available for an oxime–pyridine interaction in the database. It should be noted that it may not be possible to draw direct inferences about intermolecular bond 'strength' based upon observed D···A distances due to the fact that many other extraneous factors also contribute to the final molecular arrangement within a crystalline solid. Nevertheless, the N···O distances observed in our co-crystals are within the range of what is expected based upon information from the published literature.

A similar search on aromatic halogen···pyridine bond distances provides average C–I···N and C–Br···N values of 2.88 Å and 3.04 Å respectively. Based on our crystal structures, the average C–I···N and C–Br···N bond distances are 2.86 Å and 2.90 Å respectively. These distances correspond to an N···X contraction of 18.3% and 10.6% compared to the combined van der Waals radii of C···I and C···Br, respectively, which demonstrates that the iodine atom is a significantly better halogen-bond donor than the bromine atom (as long as both are 'activated' to the same extent). This is also in good agreement with the electrostatic argument which shows that the σ-hole on the iodine atom carries a higher positive charge than that on the bromine atom. Moreover, iodine atoms form C–I···$N_{(py)}$ primary halogen bonds with the most basic pyridine nitrogen in 4/6 cases, whereas bromine forms C–Br···$N_{(py)}$ halogen bond in only 2/6 instances. Bromine interacts more frequently with less basic secondary acceptors, *i.e.* 'O' and 'N_{azo}' 4/6 times, whereas iodine does so only 2/6 times.

Five of the six 3,3′-azobipyridine co-crystals exhibit OH···$N_{(py)}$ interactions involving the best acceptor leading to supramolecular trimers. The trimers are then linked into 2-D corrugated sheets *via* weaker interactions between I/Br with a secondary acceptor such as an oxygen atom. Thus, in this group of structures, hydrogen bonds dominate over halogen bonds, *i.e.* HB > XB (5/6) (Scheme 4). An outlier in this series is **3,3′-azpy:O*x*-I**, where the XB donor interacts preferentially with the $N_{(py)}$ acceptor. As a result, the 'free' oxime moiety forms a dimer with an oxime from a neighbouring molecule leading to infinite 1-D chain-like structure.[25]

In contrast, in five out of six 4,4′-azobipyridine co-crystals 1-D chains are obtained *via* simultaneous O–H···$N_{(py)}$ hydrogen bonds and C–X···$N_{(py)}$ (X = I/Br) halogen bonds. In this group, both donors seem to be of equal importance in the primary assembly process, *i.e.* HB ≅ XB (5/6) (Scheme 4). There is no distinction between bromine and iodine as a halogen-bond donor in any of the co-crystals. The only outlier in the series is **4,4′-azpy:O*x*-Br** where oxime···pyridine hydrogen bonds drive the formation of the co-crystal *i.e.* HB > XB (1/6) (Scheme 4). It is interesting to note the appearance of an unusual C–Br···$N_{(azo)}$ halogen bond in this structure. This observation does introduce the possibility for a new prospective acceptor site (azo nitrogen) that could be further explored in new strategies for directed assembly of complex supramolecular architectures.

Our results, which show a close competition between XB and HB donors are consistent with the work of Resnati and co-workers who designed a competitive experiment by combining 1,2-bis(4-pyridyl)-ethane (BPE) as a symmetric acceptor, 1,4-diiodotetrafluorobenzene (DITFB) as halogen-bond donor and hydroquinone (HQ) as hydrogen-bond donor in a single-pot.[26] Selective halogen-bonded co-crystal formation was observed, leaving the hydrogen-bond donor in a solution. The result suggests suitable XB donors can compete with certain HB donors and preferentially bind to the acceptor to give stable binary co-crystals. These results complement work by Cho *et al.*[27] and Bruce *et al.*[28] who designed liquid crystals using a combination of both halogen as well as hydrogen bonds affixed on the same backbone.

There is a clear distinction between the primary molecular recognition events in the two classes of azobipyridine co-

Table 6 Summary of the main structural features in 3,3′- and 4,4′-azobipyridine co-crystals of dicarboxylic acids[a]

	COOH-I (acid-H)	COOH-Br (acid-H)	OH-I (phenol-H)	OH-Br (phenol-H)	O*x*-Br (oxime-H)	O*x*-I (oxime-H)
3,3′-azpy	OH > I A	OH > Br A	OH > I A	OH > Br A	OH_{ox} > Br A	OH_{ox} < I C
4,4′-azpy	OH = I B	OH = Br B	OH = I B	OH = Br B	OH_{ox} > Br A	OH_{ox} = I B

[a] A: HB > XB, B: HB ≅ XB, C: HB < XB.

crystals with same co-formers. In one case, hydrogen bonding is the preferred interaction whereas in the other case HB and XB seem to be of equal importance. This difference cannot be explained on the basis of an electrostatically-based argument on the acceptor molecules, since the charges on the nitrogen atoms in the two azobipyridines differ only by a couple of kJ mol^{-1}. In order to seek a plausible explanation for the difference in binding behaviour we examined the electrostatic potentials of donor molecules as well as packing coefficients and melting point trends in the two classes of co-crystals.

Electrostatic surface potential calculations

Geometry optimizations were carried out and molecular electrostatic potential surfaces, MEPS were evaluated on six bi-functional donor molecules using Spartan, 2010 (Wave function, Inc. Irvine, CA). Calculations were done using both semi-empirical (PM3) and DFT methods (B3LYP, 6-31++G** basis set). Table 7 summarizes the outcome of theoretical calculations.

Despite numerical differences, both methods produced the same trends with regards to the decreasing charge on the acidic hydrogen atom on the three HB donor moieties according to the following; phenol > acid > aldoxime. These values also accurately reflect hydrogen-bond parameters for common functional groups reported previously.[29] As expected, both methods also show larger positive values for the potential surface of the σ-hole on iodine compared to that on bromine. Unfortunately, the MEPS values do not offer any additional insight as to why co-crystals of 3,3-azpy are constructed mostly through hydrogen-bonds whereas the 4,4′-azpy co-crystals are synthesized through a simultaneous use of both XB and HB interactions.

Packing coefficients and melting points

Packing coefficients were calculated for all 12 co-crystals using the Olex2 v1.2 software, Tables 8 and 9.

The packing coefficients for the two classes of co-crystals range from 66–74% and they show very similar values with the same donor molecule. The structural outlier in the first family, **3,3′-azpy:O*x*-I**, has a packing coefficient that is well within the range of the other five structures, and the structural outlier in the second family, **4,4′-azpy:O*x*-Br**, is similarly unremarkable in this context. Furthermore, as neither family (nor associated outlier) displayed any exceptional melting points, it is unlikely that a deeper analysis of weaker interactions or packing modes can explain the general differences in molecular recognition events that dominate in the two groups of co-crystals.

Since theoretical calculations, packing coefficients and melting points could not be used to explain the differences in binding events, this 'synthon crossover',[30] could be rationalized based on the difference in binding site orientation in the two azobipyridine molecules.

The nitrogen atoms on 3,3′-azobipyridine have an anti-parallel orientation with respect to each other (Scheme 1). This geometry does not favour the ready formation of 1-D chains as the lack of ideal complementary means that adjacent molecules need to be forcefully brought in close proximity at angles that can enforce a 1-D assembly formation. In doing so the overall energy of the system may increase while its stability is compromised. On the other hand, forming discrete trimers is less challenging and requires no considerable effort. These trimers can be readily connected *via* secondary interactions thus leading to a stable structure. Under these conditions, the HB donor (which is a somewhat more competitive donor moiety) binds to the best acceptor site, *i.e.* the pyridine nitrogen, leading to a stable trimer. I/Br then interacts with the next best acceptor (oxygen/azo nitrogen) linking the trimers into a 2-D architecture.

In 4,4′-azobipyridine however, the binding sites are co-linear which naturally favours the formation of infinite 1-D chains with no significant loss in energy. Under these conditions, the acceptor nitrogen atom binds to an XB donor as quickly as it binds to HB donor producing 1-D infinite chains constructed form alternative D–H···A and X···A interactions. The take home message from this analysis is that thermodynamically favoured supramolecular assemblies (the 3,3′-azpy co-crystals) have time to maximize intermolecular interactions and therefore the HB donors 'win' over the XB donors. However, the facile and rapid formation of more linear 1-D chains in the 4,4′-azpy co-crystals represent kinetic products and in this case there is a 50 : 50 chance that each bipy will be connected to an XB and HB donor simultaneously which is what is observed in five of the six co-crystals.

We have established that the orientation of the binding site in the acceptor can influence supramolecular assembly in very specific ways, and several points can be made based on the crystal structure analysis for 3,3′- and 4,4′-azobipyridine co-crystals:

1) In 3,3′-azpy co-crystals hydrogen bonding is the primary driving force (HB > XB), while in 4,4′-azpy co-crystals both

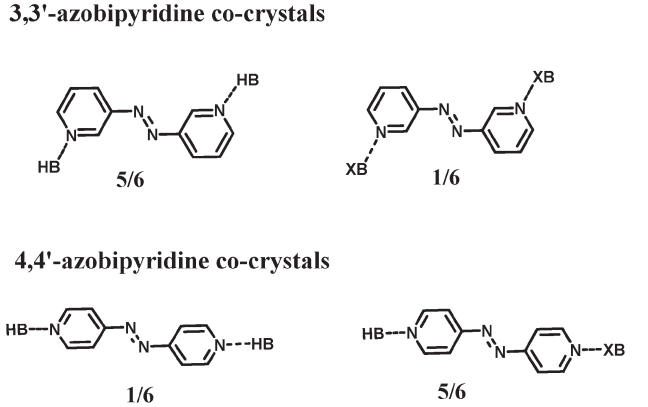

Scheme 4 Overview of the structural landscape 3,3′- and 4,4′-azobipyridine co-crystals.

Table 7 Electrostatic surface potentials expressed as charges in kJ mol^{-1}

	COOH-I		COOH-Br		OH-I		OH-Br		O*x*-I		O*x*-Br	
	H	I	H	Br	H	I	H	Br	H	I	H	Br
PM3	144	222	144	160	156	202	163	152	134	204	135	147
DFT	296	166	305	142	305	155	314	121	283	153	276	129

Table 8 Packing efficiency and mp of 3,3′-azpy co-crystals

	COOH-I	COOH-Br	OH-I	OH-Br	Ox-I	Ox-Br
Packing coefficient (%)	74	69	68	71	69	69
Melting points (°C)	182–185	155–157	125–127	170–173	145–148	105–108

Table 9 Packing efficiency and mp of 4,4′-azpy co-crystals

	COOH-I	COOH-Br	OH-I	OH-Br	Ox-I	Ox-Br
Packing coefficient (%)	74	76	67	69	66	67
Melting points (°C)	220–222	190–191	163–165	133–136	115–116	125–126

hydrogen as well as halogen bonds equally contribute in the assembly process (HB ≅ XB).

2) Among the halogen atoms, iodine is a better halogen-bond donor than bromine.

3) There is no distinction between three types of hydrogen-bond donors (–COOH, –OH and –CN(R)OH) in terms of binding to the azobipyridines in the presence of halogens.

It is clear that more work is needed to tease out the precise reason behind the observed patterns of behavior in these two ditopic acceptors, and we have therefore embarked on a study of comparable symmetric ditopic N-acceptors that offer the same type of geometric differences that 3,3′- and 4,4′-azop display. The fact that HB and XB strengths are comparable (and these interactions are both reversible and interchangeable) means that it may not always be possible to identify the exact cause–effect relationship until a much larger amount of data has been generated and analyzed.

Acknowledgements

We are grateful for financial support from the NSF (CHE-0957607).

Notes and references

1 (*a*) R. D. B. Walsh, M. W. Bradner, S. Fleischman, L. A. Morales, B. Moulton, N. Rodriguez-Hornedo and M. J. Zaworotko, *Chem. Commun.*, 2003, 186–187; (*b*) M. Wenger and J. Bernstein, *Angew. Chem., Int. Ed.*, 2006, **45**, 7966–7969; (*c*) J.-M. Lehn, *Science*, 2002, **295**, 2400; (*d*) G. R. Desiraju, *Acc. Chem. Res.*, 2002, **35**, 565–573.

2 (*a*) C. B. Aakeröy, J. F. Urbina and J. Desper, *Chem. Commun.*, 2005, 2820–2822; (*b*) T. R. Shattock, K. K. Arora, P. Vishweshwar and M. J. Zaworotko, *Cryst. Growth Des.*, 2008, **8**, 4533–4545; (*c*) C. B. Aakeröy, I. Hussain, S. Forbes and J. Desper, *CrystEngComm*, 2007, **9**, 46–54; (*d*) B. R. Bhogala and A. Nangia, *Cryst. Growth Des.*, 2003, **3**, 547–554.

3 (*a*) P. Vishweshwar, J. A. McMahon, M. L. Peterson, M. B. Hickey, T. R. Shattock and M. J. Zaworotko, *Chem. Commun.*, 2005, 4601–4603; (*b*) C. B. Aakeröy, J. Desper and B. A. Helfrich, *CrystEngComm*, 2004, **6**, 19–24; (*c*) L. S. Reddy, A. Nangia and V. M. Lynch, *Cryst. Growth Des.*, 2004, **4**, 89–94; (*d*) C. B. Aakeröy, A. M. Beatty, B. A. Helfrich and M. Nieuwenhuyzen, *Cryst. Growth Des.*, 2003, **3**, 159–165.

4 (*a*) K. S. Huang, D. Britton, M. C. Etter and S. R. Byrn, *J. Mater. Chem.*, 1997, **7**, 713; (*b*) L. R. MacGillivray, J. L. Reid and J. A. Ripmeester, *J. Am. Chem. Soc.*, 2000, **122**, 7817; (*c*) T. Friščić and L. R. McGillivray, *Chem. Commun.*, 2009, 773–775; (*d*) I. D. H. Oswald, W. D. S. Motherwell and S. Parsons, *Acta Crystallogr.*, 2004, **60**, 1967–1969; (*e*) P. S. Wheatley, A. J. Lough, G. Ferguson and C. Glidewell, *Acta Crystallogr.*, 1999, **55**, 1489–1492; (*f*) A. Mukherjee and G. R. Desiraju, *Chem. Commun.*, 2011, **47**, 4090–4092.

5 C. B. Aakeröy, D. J. Salmon, M. M. Smith and J. Desper, *Cryst. Growth Des.*, 2006, **6**, 1033–1042.

6 (*a*) P. Metrangolo, T. Pillati, G. Resnati and A. Stevenazzi, *Chem. Commun.*, 2004, 1492–1493; (*b*) P. Metrangolo, T. Pilati and G. Resnati, *CrystEngComm*, 2006, **8**, 946–947; (*c*) K. Raatikainen and K. Rissanen, *CrystEngComm*, 2011, **13**, 6972–6977; (*d*) P. Politzer and J. S. Murray, *Chem. Halides, Pseudo-Halides Azides*, 1995, **Pt. 1**, 1–30; (*e*) T. Brinck, J. S. Murray and P. Politzer, *Int. J. Quantum Chem., Quantum Biol. Symp.*, 1992, **19**, 57–64.

7 P. Auffinger, F. A. Hays, E. Westhof and P. S. Ho, *Proc. Natl. Acad. Sci. U. S. A.*, 2004, **101**, 16789–16794.

8 A. R. Voth and P. S. Ho, *Curr. Top. Med. Chem.*, 2007, **7**, 1336–1348.

9 G. M. Espallargas, *Ideas Chem. Mol. Sci.: Adv. Nanotechnol., Mater. Devices*, 2010, 115–138.

10 P. Metrangolo, H. Neukirch, T. Pilati and G. Resnati, *Acc. Chem. Res.*, 2005, **38**, 386–395.

11 (*a*) C. B. Aakeröy, J. Desper and M. M. Smith, *Chem. Commun.*, 2007, 3936; (*b*) M. C. Etter, *J. Phys. Chem.*, 1991, **95**, 4601; (*c*) M. C. Etter, *Acc. Chem. Res.*, 1990, **23**, 120.

12 J. W. Steed and J. L. Atwood, *Supramolecular Chemistry*, John Wiley and Sons, Ltd., 2nd edn, 2009.

13 P. Metrangolo, H. Neukirch, T. Pilati and G. Resnati, *Acc. Chem. Res.*, 2005, **38**, 386–395.

14 *Halogen Bonding: Fundamentals and Applications*, ed. P. Metrangolo and G. Resnati, Structure and Bonding, Springer, Berlin, 2008, 126.

15 (*a*) C. B. Aakeröy, N. Schultheiss, A. Rajbanshi, J. Desper and C. Moore, *Cryst. Growth Des.*, 2009, **9**, 432; (*b*) C. B. Aakeröy, M. Fasulo, N. Schultheiss, J. Desper and C. Moore, *J. Am. Chem. Soc.*, 2007, **129**, 13772; (*c*) C. B. Aakeröy, J. Desper, B. A. Helfrich, P. Metrangolo,

T. Pilati, G. Resnati and A. Stevenazzi, *Chem. Commun.*, 2007, 4236.
16 (*a*) C. B. Aakeröy, A. Rajbanshi, Z. J. Li and J. Desper, *CrystEngComm*, 2010, **12**, 4231–4239; (*b*) C. B. Aakeröy, J. Desper and M. E. Fasulo, *CrystEngComm*, 2006, **8**, 586–588.
17 C. B. Aakeröy, S. Panikkattu, B. DeHaven and J. Desper, *CrystEngComm*, 2013, **15**, 463–470.
18 C. B. Aakeröy, P. D. Chopade, C. Ganser and J. Desper, *Chem. Commun.*, 2011, **47**, 4688–4690.
19 C. B. Aakeröy, A. S. Sinha, K. Epa, C. L. Spartz and J. Desper, *Chem. Commun.*, 2012, **48**, 11289–11291.
20 APEXII v2009. 5–1, © 2009, Bruker Analytical X-ray Systems, Madison, WI.
21 COSMO v1. 60, © 1999–2009, Bruker Analytical X-ray Systems, Madison, WI.
22 SAINT v7. 60a, © 1997–2008, Bruker Analytical X-ray Systems, Madison, WI.
23 SADABS v2008/1, © 2008, Bruker Analytical X-ray Systems, Madison, WI.
24 SHELXTL v2008/4, © 2008, Bruker Analytical X-ray Systems, Madison, WI.
25 (*a*) A. D. Ward, V. R. Ward and E. R. T. Tiekink, *Z. Kristallogr. - New Cryst. Struct.*, 2001, **216**, 563; (*b*) E. Arte, J. P. Declercq, G. Germain and M. V. Meerssche, *Bull. Soc. Chim. Belg.*, 1980, **89**, 155; (*c*) B. Jerslev and S. Larsen, *Acta Chem. Scand.*, 1992, **46**, 1195; (*d*) M. Tonogaki, T. Kawata, S. Ohba, Y. Iwata and I. Shibuya, *Acta Crystallogr., Sect. B: Struct. Sci.*, 1993, **49**, 1031.
26 E. Corradi, S. V. Meille, M. T. Messina, P. Metrangolo and G. Resnati, *Angew. Chem., Int. Ed.*, 2000, **39**, 1782–1785.
27 C. M. Cho, X. Wang, J. J. Li, C. He and J. Xu, *Liq. Cryst.*, 2012, 1–12.
28 C. Präsang, H. L. Nguyen, P. N. Horton, A. C. Whitwood and D. W. Bruce, *Chem. Commun.*, 2008, 6164–6.
29 M. H. Abraham and J. A. Platts, *J. Org. Chem.*, 2001, **66**, 3484–3491.
30 C. B. Aakeröy, P. D. Chopade and J. Desper, *Cryst. Growth Des.*, 2011, **11**, 5333–5336.

